Materials Science and Engineering B 322 (2025) 118581

Contents lists available at ScienceDirect

Materials Science & Engineering B

journal homepage: www.elsevier.com/locate/mseb

Quartz crystal microbalance modified with rhodamine-polyacrylonitrile nanofibers for acetone vapor sensing

Rifat Capan [a,*], Inci Capan [a], Mevlut Bayrakci [b]

[a] Balikesir University, Science&Literature Faculty, Physics Department, 10145 Balikesir, Turkey
[b] Karamanoglu Mehmetbey University, Engineering Faculty, Bioengineering Department, 70200 Karaman, Turkey

ARTICLE INFO

Keywords:
Polyacrylonitrile
Acetone
Vapor sensor
Nanofiber
Pseudo first-order model
Elovich model
Density functional theory

ABSTRACT

Rhodamine based polyacrylonitrile (PAN-RHE) electrospun nanofiber sensor was used to investigate for the vapor sensor application against acetone, ethanol, and benzene vapors at room temperature. Quartz crystal microbalance technique was employed to collect the time-dependent sensor response data which were analyzed for the determination of sensor parameters and for the investigation of the adsorption behavior between nanofiber and vapor molecules. The acetone vapor yielded the highest response with a best response with a sensitivity of 0.0243 Hz/ppm. The limit of detection and limit of quantification for acetone vapor were determined as 135.80 ppm and 411.52 ppm, respectively. Pseudo first-order and Elovich models were chosen to investigate adsorption dynamics. Pseudo first-order adsorption rate and Elovich desorption constant were calculated using time-dependent data. A possible hydrogen binding or dipole–dipole interaction between the vapor molecules and rhodamine and/or nitrile units of the PAN fiber chain was proposed as a sensor interaction mechanism.

1. Introduction

Rapid technological developments, the desire of people to live a high-level of welfare, the rapid growth of cities and many other factors have caused damage to the environment. They confronted the world with face the threat of climate change, environmental pollution, and global warming as well as health of living beings and the future of our world [1,2]. Climate change and temperature rise would have a devastating impact and to minimize these changes, multiple actions on greenhouse gas emissions are urgently needed to be addressed. It is clear that a number factors (industry, heating, traffic etc.) and several pollutants (organic and/or inorganic gases, particles etc.) play a role in these unwanted changes. When toxic chemicals vaporize as harmful gases, they create several problems.

If volatile organic compounds (VOCs), a class of volatile carbon compounds, are exposed to sunlight, atmospheric photochemical reactions will occur depending on the type and amount of VOCs emitted. These chemical reactions disrupt ecosystems and have crippling effects on both the environment and human beings [3,4]. VOCs have a variety of sources, including: gasoline-burning engines and cars, consumer products such as paint, insecticides, cleaners, industrial solvents and chemical manufacturing. When inhaled or absorbed by living organisms, they cause many health problems or damage such as airway irritation, lungs, central nervous system (CNS), kidneys and liver. Aerosols, solvents, exhaust streams used in unventilated areas can generate dangerous toxins. If they are exposed to high quantities, humans can experience dizziness, headaches, memory loss and visual impairment. Some of them have carcinogenic properties which could lead to long-term and possibly fatal conditions [5]. Acetone, ethanol, and benzene vapors were chosen in this study because they are extensively being used in our daily life, transportation, chemical, biomedical, pharmaceutics, food industries and laboratories as a solvent, dissolve plastics, cleaning agent, purify paraffin and dehydrate tissues, motor vehicles, alcohols etc. They are playing an unfavorable role for climate change, environmental pollution, global warming, and the health of living beings. The Threshold limit value (TLV) is defined as the maximum concentration of a chemical permitted during a working day (8 h) and is the supposed limit that a person can be exposed to a certain VOC without experiencing adverse effects. TLV values were determined as 750 ppm for acetone, 1 ppm for benzene, and 1000 ppm for ethanol vapors [6,7]. The inhalation of acetone can cause irritation of the eyes, throat, nose, fatigue, nausea, dizziness, headache, muscle weakness, drowsiness, loss of coordinated

* Corresponding author.
E-mail addresses: rcapan@balikesir.edu.tr (R. Capan), inci.capan@gmail.com (I. Capan), mevlutbayrakci@gmail.com (M. Bayrakci).

https://doi.org/10.1016/j.mseb.2025.118581
Received 14 May 2025; Received in revised form 22 June 2025; Accepted 3 July 2025
Available online 7 July 2025

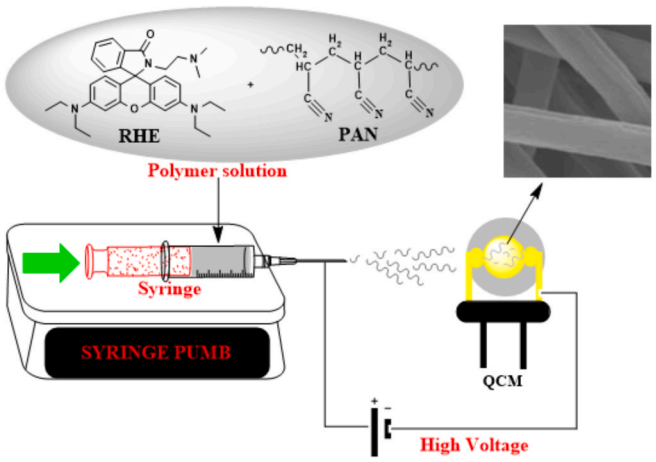

Fig. 1. The electrospinning setup for the preparation of nanofiber sensor PAN-RHE.

speech, and harmfulness to the nerve system [8]. Benzene is of particular concern because of its toxicity and carcinogenic properties. It is a carcinogen via all routes of exposure and is well known to be a major cause of leukemia and lymphomas. Inhaling benzene in air with a high level of concentration may be fatal due to respiratory failure [9]. Ethanol vapor can cause health problems such as irritation of eyes, drowsiness, headache, and difficulty in breathing [10]. It is a well-known fact that this substance is used as a beverage and is one of the main causes of traffic accidents. Therefore, it is vital that ethanol vapor is detected at ppm levels. This is not only for medical use, but also to solve a social problem. As a result of these reasons, it is necessary to control these vapor concentrations in our daily life to have a livable environment, healthy life, and safe workplace.

Some scientific studies on sensor materials have been continuing rapidly in order to minimize the damage to the environment and to ensure that the world becomes a livable place [11]. It is inevitable to prevent global warming by minimizing air pollution, which is a part of environmental pollution. For this reason, the sensor research has focused on fabricating well-defined nanostructure sensor materials with a controlled morphology and structural architecture as well as new advantageous functional groups to enhance molecular sensing performances for a higher stability, selectivity, and sensitivity value [12] such as a liquid crystal for acetone [13], a metal–organic framework (MOF) for benzene [14] and a polyvinylpyrrolidone (PVP) nanofiber for ethanol [15]. In the recent years, nanofiber materials fabricated by electrospinning method onto a quartz crystal substrate have been preferred to use in the sensor application field because of their large surface area to volume ratio, high porosity, high adsorption and fast desorption capabilities, good chemical, mechanical and physical stability properties [16]. Various polyacrylonitrile (PAN) based nanofibers deposited onto a quartz crystal substrate were recently studied for the detection of organic vapors. Some recent studies can be summarized as a PAN nanofiber [17], a polyacrylonitrile (PAN)/polypyrrole (PPy) nanofiber [18], polyacrylonitrile (PAN) nanofiber mixed with citric acid (CA) [19], the PAN nanofiber sensor was overlaid with chitosan [20], polyacrylonitrile/nickel nanofibers [21] and the rhodamine-based PAN nanofiber [22,23]. A highly mass change sensitive in nanogram scale Quartz crystal microbalance (QCM) method is attracting significant attention due to low cost, portable and easy operations. It allows us to monitor any mass changes when sensitive nanofiber material adsorbs a vapor molecule. Therefore, this technique is suitable for examining the organic vapor adsorption properties. In the literature, many models namely Elovich, Pseudo, Freundlich, Langmuir and Langmuir-Freundlich models were used to analyze the adsorption dynamics and the adsorption coefficient, adsorption rate and correlation coefficients can be determined [15,24,25]. Our two recent studies were concentrated on the sensor behavior of PAN nanofiber with the rhodamine-based (the nanofiber sensor PAN-RHE) onto a mass-sensitive quartz crystal substrate using the electrospinning method against chlorinated hydrocarbon vapors. Rhodamine has a good molecular structure for binding of the toxic gases due to the presence of excellent electron-donating and accepting sides [22,23].

Although some significant research progresses in acetone and ethanol vapors detection using PAN nanofiber sensor were achieved [26–28], there are limited studies on the detection of these vapors using QCM PAN nanofiber sensor by measuring QCM method. Therefore, the present study is the first investigation of the nanofiber sensor PAN-RHE properties against acetone, ethanol, and benzene vapors. All sensor parameters such as stability, selectivity, sensitivity, reproducibility, the response and recovery times, limit of detection (LOD), the limit of quantification (LOQ) parameters were determined using the real-time QCM kinetic measurements. The Elovich and Pseudo adsorption models were selected to investigate the adsorption behavior of the nanofiber sensor PAN-RHE to obtain the adsorption rate constant, the equilibrium density, and the correlation coefficient of the nanofiber sensor PAN-RHE.

2. Experimental details

This section provided details on the preparation of the nanofiber sensor PAN-RHE, the experimental QCM measurement system, and the impact of relative humidity (RH) on the QCM gas sensing response of the PAN-RHE sensor. The experiments were conducted under 25 % RH and 80 % RH conditions at a temperature of 25 °C.

2.1. Preparation process of the nanofiber sensor PAN-RHE

PAN was dissolved in dimethylformamide (DMF) using a magnetic stirrer overnight at room temperature to obtain a homogeneous polymeric solution (10 % w/v). PAN nanofibers were deposited on the QCM surface using an electrospinning apparatus with the setup as depicted in Fig. 1. The PAN solution was loaded into a syringe with 0.7 mm inner diameter and connected to a high voltage power supply for the electrospinning process. It was electrospun at an approximate feed rate between 1–1.5 mL h^{-1} with a working distance of 15–20 cm and a high electric voltage of 20 kV for PAN fibers. All processes were performed at room temperature under 19 % RH. The obtained morphological and analytical results for the characterization of fiber mat were similar to the previously published data [22,23].

2.2. Characterization methods for the nanofiber sensor PAN-RHE

Scanning electron microscope (SEM) images of prepared nanofiber mats were taken by a Zeiss EVO LS10 model SEM instrument. The hydrophilicity of the membrane surface is analyzed by a contact angle meter which were obtained by Biolin Scientific Theta Lite TL101 instrument with water droplets. Geometric optimizations and theoretical calculations were verified by applying density functional theory (DFT) with B3LYP and 6-311G (d,p) basis. DFT calculations were conceded using Gaussian 09 program [29]. All chemicals used were of analytical grade, and they were used as received.

2.3. QCM measurements details

QCM system is highly sensitive to a mass change in the nanoscale and is widely used in sensor applications. When a sensor material deposited onto a QCM crystal detects a target molecule, a change of oscillation frequency occurs. It depends on the deposited mass rate which depends on physical or chemical interactions. The principal determination between this mass change and frequency change is defined by Sauerbrey as follows [30]:

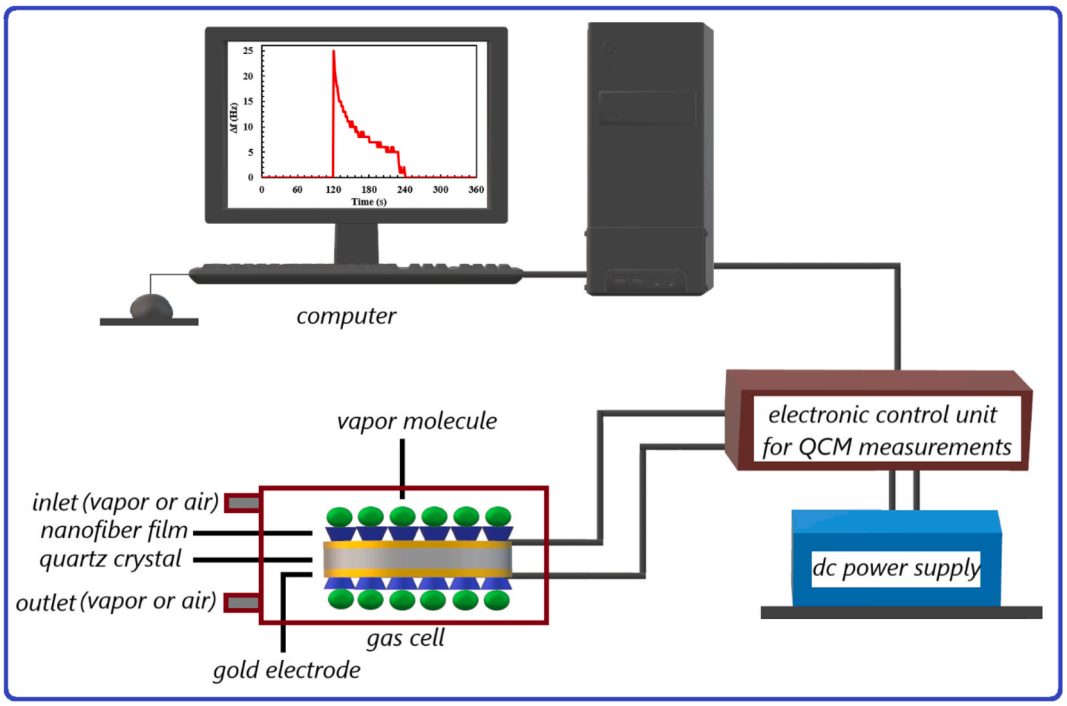

Fig. 2. A schematic diagram of QCM measurement system.

$$\Delta f = -\left(\frac{2f_0^2}{\rho_q^{1/2}\mu_q^{1/2}A}\right)\Delta m \quad (1)$$

where f_0 is the initial oscillation frequency of uncoated QCM crystal (3.5 Hz), ρ_q is the density of quartz (2.648 g cm^{-3}), μ_q is the shear modulus of quartz (2.947 $\times$ 10^{11} g cm^{-1} s^{-2}), A is the piezo-electrically active area (1.13 cm^2).

QCM system is widely used for nanofiber sensor applications to observe the mass changes by measuring the frequency changes when a sensing element is exposed to the gas or vapor [15,31,32]. In this study, a home-made computer controlled QCM measurement system illustrated in Fig. 2 was used to monitor frequency changes when the nanofiber sensor PAN-RHE was exposed to acetone, ethanol, and benzene vapors. For the vapor interaction experiments, an isolated gas cell had inlet and outlet holes that were used to control the vapor and dry air flow as a function of time. The nanofiber sensor PAN-RHE was deposited onto 3.5 MHz AT-cut quartz crystal (GTE SYLVANIA Company).

Acetone, ethanol, and benzene with purities of $\geq$ 99.0 % were supplied from Sigma-Aldrich and used as received without further purification. As each analyte is present in liquid form at the room temperature; it was easily taken in half a tube of 20 mL and heated until an equilibrium distribution was reached, resulting in the formation of saturated vapor in the other half of the tube. The saturated vapor molecules were collected into a 5 mL Hamilton syringe and injected into the gas cell for saturated concentration value of 100 %. For the kinetic studies the vapor was injected into the gas cell during a time interval of 2 min. After that, dry air was sent into the gas cell for the following 2 min. Preliminary kinetic tests on the gas sensing performance of the initial PAN-RHE sensor devices have revealed the response and the recovery times in the range of a few seconds. Therefore 2 min of time interval was found to be sufficient for the gas molecules and the PAN-RHE sensor for their interaction. Same applies for the recovery; as the dry air was injected into the gas cell dissociation of the gas molecules and the PAN-RHE molecules occupied in the range of seconds. To obtain the concentration effect and to determine the sensitivity values of the nanofiber sensor PAN-RHE, the concentration ratios (25 %, 50 %, 75 % and 100 %) of each vapor were used to inject to the gas cell. The volume of 1.25 mL (representing 25 %), 2.5 mL (representing 50 %), 3.75 mL (representing 75 %) and 5 mL (representing 100 %) of the injector was filled with saturated vapor and the rest of the injector volume was filled with dry air to maintain the concentration-dependent behavior. In order to elucidate the stability and reproducibility of the nanofiber sensor PAN-RHE against the selected vapor, the saturated concentration value of 100 % was injected to get three kinetic QCM cycles. The sensor parameters and adsorption coefficients of the nanofiber sensor PAN-RHE for acetone, ethanol and benzene vapors were determined using these kinetic QCM cycles.

The concentration value (c *in ppm*) of each vapor was calculated using Eq. (2) [33]:

$$c = \frac{22.4\rho V}{MV_0}x10^6 \quad (2)$$

where ρ is the density of selected vapor (0.791 g/mL for acetone, 0.7894 g/mL for ethanol and 0.874 g/mL for benzene at 25 °C), V is the volume of injected vapor into the gas cell (5 mL), M is the vapor molecular weight (58.08 g/mol for acetone, 46.07 g/mol for ethanol and 78.11 g/mol for benzene) and V_0 is the volume of the gas cell (1.5 mL).

2.4. Measurement of the effect of humidity

If water vapor can be transported into the gas cell via the carrier gas, any ambient water vapor present during the measurements could pose a risk to the accuracy of the spectroscopic results [34,35]. An ideal baseline signal can be performed under high vacuum conditions. When the time kinetic measurements are recorded at 25 °C, the baseline signal could possess a small drift due to water vapor molecules in the gas chamber. It is very difficult to avoid water vapor molecules during these measurements. Therefore, it is an important issue to study the humidity effect since there is the possibility for water vapor to be transported along with the carrier gas into the gas cell [36]. To minimize the effect of water vapor, a reference gas (dry air supplied commercially from industry with the value of 0.03 % RH) was used during the experiment between the nanofiber sensor PAN-RHE and the selected vapor. In our case dry air was flushed through the gas cell for 2 min. In order to

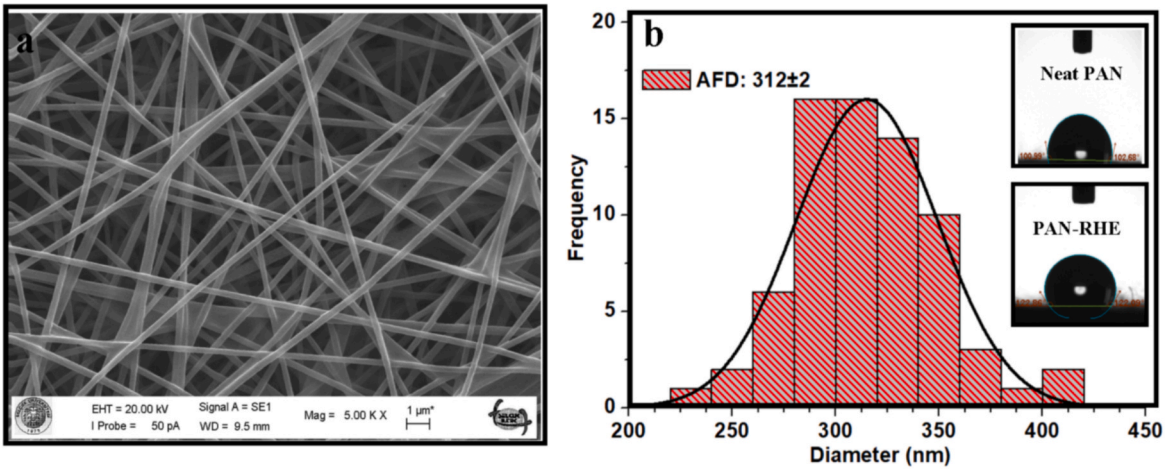

Fig. 3. (a) SEM image (b) size distribution. The inset: contact angle measurement for the nanofiber sensor PAN-RHE.

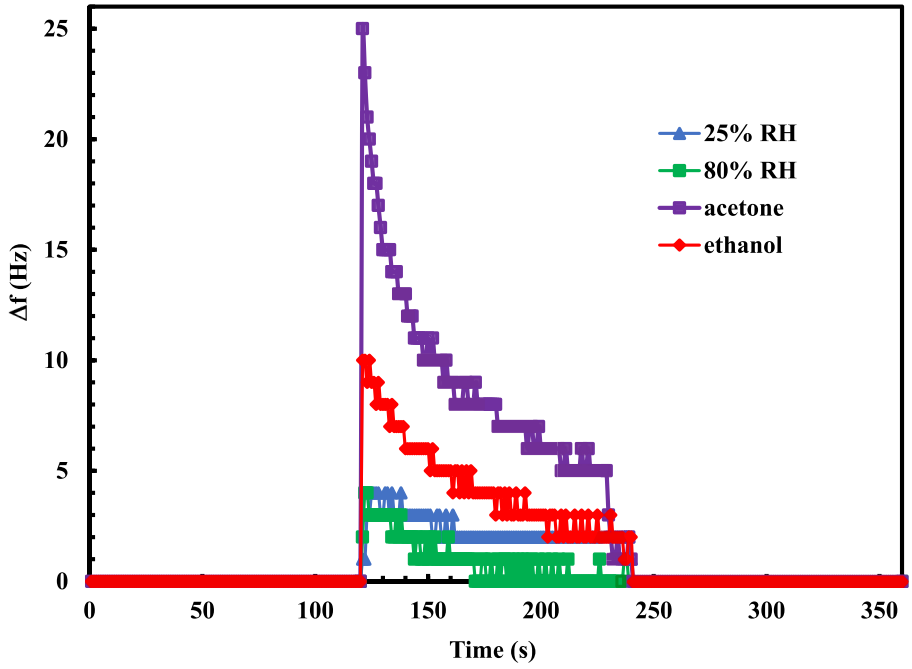

Fig. 4. The QCM measurements recorded in 25% and 80% RH values during exposure to acetone and ethanol vapors.

investigate the relative humidity effect on the selected vapor response properties, time dependent QCM measurements were recorded for the laboratory conditions at 25 °C with the values of 25 % and 80 % RH. RH value was controlled by mixing the dry air with a wet air containing saturated vapor at 25 °C. Continuous humidity monitoring and control of the gas testing environment during all experimental steps were monitored by an HTC-2 LCD Digital Thermometer Hygrometer.

3. Results and discussions

3.1. Morphological characterization of the nanofiber sensor PAN-RHE

The surface morphological structure of the fiber matrix was analyzed using a scanning electron microscope. For SEM imaging, the fiber matrix were adhered to a holder with carbon tape and covered with a layer of gold. The samples were then examined under a microscope and their images were taken. The average fiber diameter was analyzed by studying the SEM photos with Image J software. The morphological characterization of PAN-RHE nanofibers was explored by SEM measurement. SEM results of the electrospun fibers obtained from the PAN solutions with RHE were shown in Fig. 3.

From the SEM image of PAN-RHE fibers (Fig. 3a), it was clearly seen that fiber matrix having smooth surface morphology with bead-free was formed. While all of the fiber matrix were mostly uniform in the fiber skeleton, any crystals belonging to RHE structures were not encountered. This situation is probably due to small size and homogeneous distribution of RHE in the fiber matrix (Fig. 3a). From the SEM results, it was observed that average diameter of the PAN nanofiber with RHE was seen around 312 nm (Fig. 3b). Comparing the fiber diameters of pure PAN [37,38] and/or PAN-RHE, slightly increase in fiber diameters of PAN-RHE is probably due to presence of the RHE on the fiber matrix. The surface wettability of the PAN and PAN-RHE nanofibers was studied using contact angle measurements. As shown the inset in Fig. 3b, it was found that the contact angle increased from 102° to 122° with RHE content in the PAN. This is due to the presence of the apolar phenyl rings of RHE [22]. This increase in the contact angle measurements indicated

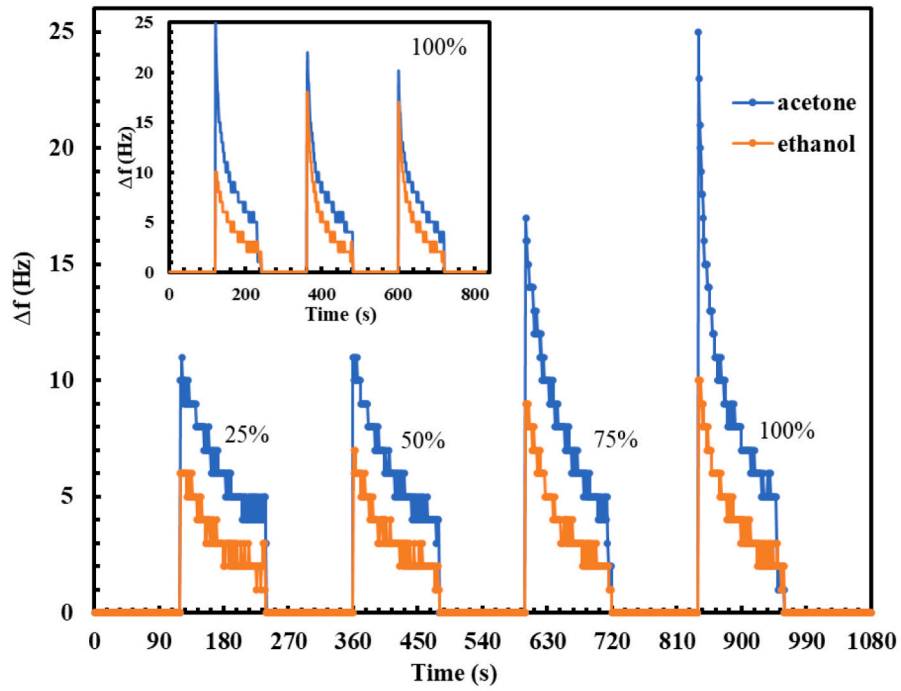

(a)

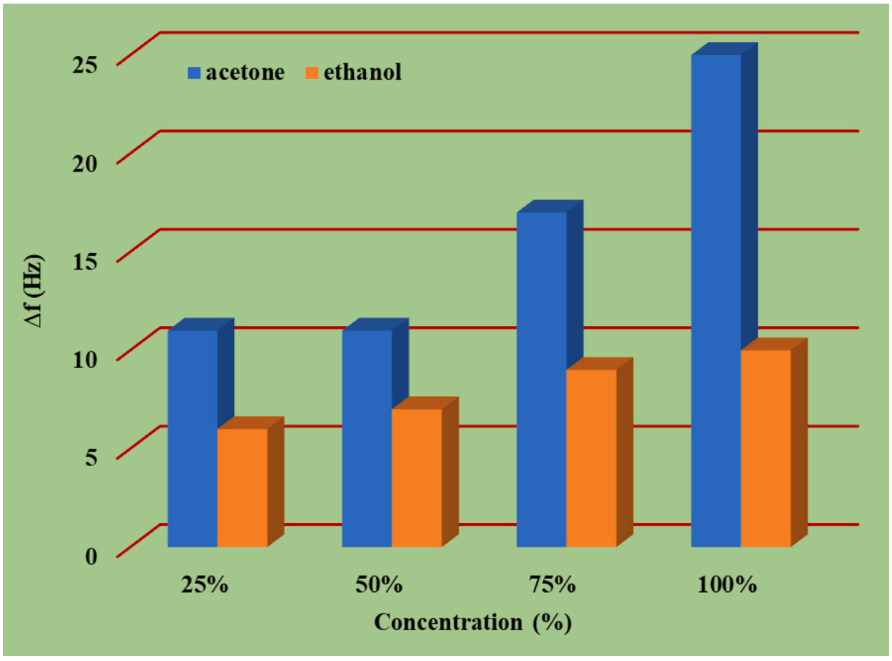

(b)

Fig. 5. The response of the nanofiber sensor PAN-RHE (a) Δf versus t (b) Δf versus c at the different concentration (c) Δf versus c at the constant concentration.

that a rhodamine based polyacrylonitrile fiber mat with a hydrophobic surface was obtained.

3.2. The effect of humidity on the PAN-RHE nanofiber sensor

If the water molecules in the atmosphere affect this interaction, then the sensitivity to humidity becomes one of the major drawbacks in the application of the VOCs sensor using the QCM measurement [39]. In order to investigate the relative humidity effect on the nanofiber sensor PAN-RHE, two values (25 % RH and 80 % RH) were selected with the maximum difference achievable under our laboratory conditions. Equal amounts of wet air (25 % RH and 80 % RH), acetone and ethanol vapors were separately injected into the gas cell using a 5 mL HAMILTON syringe. The nanofiber sensor PAN-RHE was allowed to interact for 2 min, then the gas cell was flushed with the dry air to allow the recovery of the nanofiber sensor PAN-RHE. The sensing mechanism in QCM system relies on the detection of the frequency changes caused by a change in deposited mass onto the nanofiber sensor PAN-RHE due to the

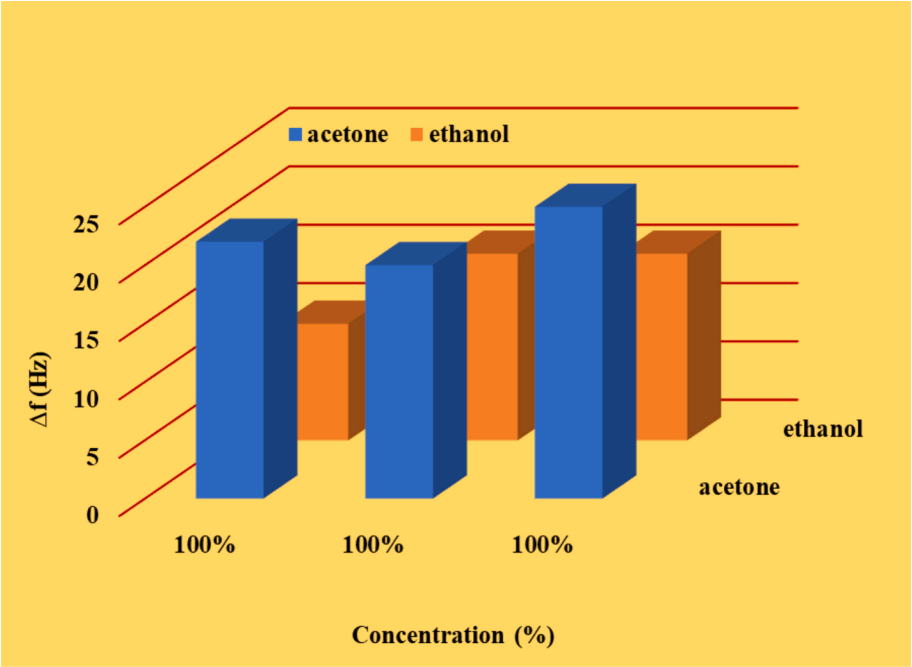

(c)

Fig. 5. (*continued*).

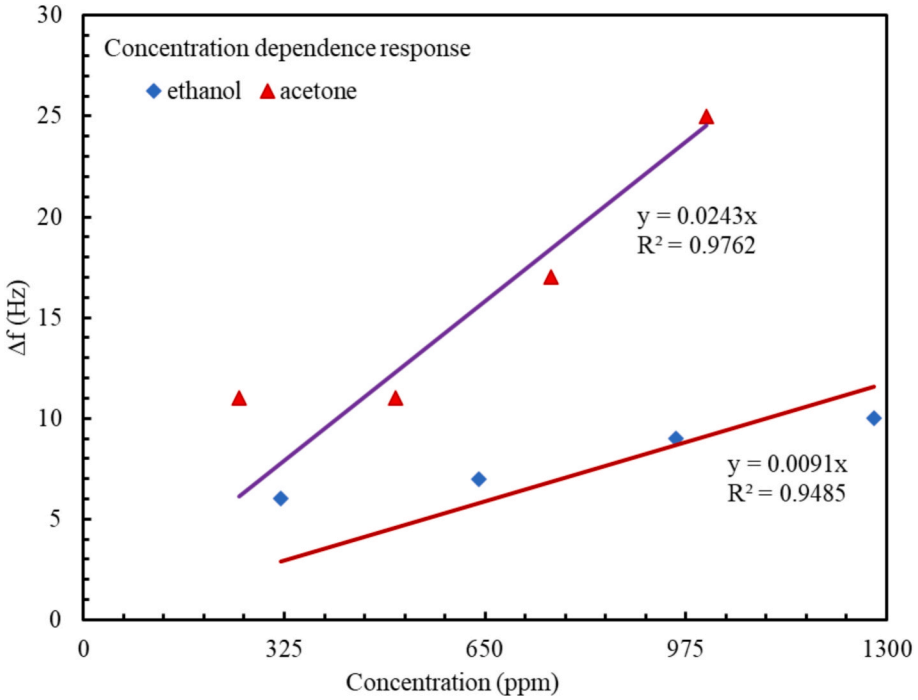

Fig. 6. Calibration curves for ethanol and acetone vapors.

interaction between the sensor element and vapor molecules. This interaction occurs by the adsorption of the vapor molecules onto the nanofiber sensor PAN-RHE structure.

The responses of the nanofiber sensor PAN-RHE to wet air, acetone and ethanol vapors were shown in Fig. 4. After being injected into the gas cell for approximately 120 s, the gas cell was flushed with the dry air to the recovery of the PAN-RHE nanofiber.

If water molecules in the atmosphere interact with the nanofiber sensor PAN-RHE, the frequency shift should have a significant change compared with the vapor molecules. According to our results in Fig. 4, the relative humidity of the air only had a minimal effect in the gas sensing response, and this effect was negligible when the PAN-RHE nanofiber was exposed to vapors. Similar results can be seen in the literature for other sensor materials [22,40,41].

3.3. Vapor sensor behavior of the nanofiber sensor PAN-RHE

Frequency shift (Δf) is defined in Eq. (2), and it was found as the

Table 1
The sensor parameters of the nanofiber sensor PAN-RHE exposed to different vapors.

	S(Hz/ppm)	*LOD*(ppm)	*LOQ*(ppm)	Reference
Chloroform	0.0276	119.56	362.31	22
Trichloroethylene	0.0151	218.54	662.25	
Carbon tetrachloride	0.0201	164.17	497.51	
Dichloromethane	0.0215	153	465	23
Acetone	0.0243	135.80	411.52	This study
Ethanol	0.0091	362.63	1098.9	This study

Table 2
The existing acetone vapor sensors.

Acetone	*S*(Hz/ppm)	*LOD*(ppm)	*LOQ*(ppm)	Reference
The nanofiber sensor PAN-RHE	0.0243	135.80	411.52	This study
Citric acid (CA) and chitosan (CS) in polyacrylonitrile (PAN) nanofibers	0.015	not reported	not reported	44
MOF-based QCM sensor	0.114	not reported	not reported	45
Metal organic framework (MOF) MIL-101(Cr)	0.090	not reported	not reported	46
amino morpholine schiff base functionalized calix[4]arene cage	1.16	not reported	not reported	24
Calix[4]arene Thiourea Decorated with 2-(2 Aminophenyl)benzothiazole	0.039	85 ppm	256 ppm	47
N-cyclohexylmethacrylamide LB thin films	0.044	67.72	not reported	48

Table 3
The physical properties of acetone and ethanol vapor.

VOC	Molar mass (g/mol)	Density (g/mL at 25 °C)	Vapor pressure (kPa at 25 °C)	Viscosity (mPa s at 25 °C)	Dipole moment (D)
Acetone	58.08	0.791	30.6	0.306	2.88
Ethanol	46.07	0.789	7.828	1.074	1.69

difference between the frequency of the baseline (f_0) and the observed frequency (f) during each injected concentration cycle.

$$\Delta f = (f - f_0) \tag{3}$$

In general, the reversible process in a sensor application is called a three-step dynamic process which are adsorption, diffusion, and desorption processes [17]. When the vapor molecules come into contact with a sensor material, a rapid increase occurs in Δf because of the adsorption effect. When dynamic equilibrium is established, the number of adsorbed molecules is equal to the number of desorbed molecules and Δf attains a steady-state value. If a fresh air is injected into the gas cell, the desorption process starts and a rapid decrease in Δf value returns to the initial state.

The sensing behavior of the nanofiber sensor PAN-RHE on acetone, ethanol and benzene vapors were investigated systematically by monitoring the frequency shifts in the nanofiber sensor PAN-RHE. The response and recovery behavior of the sensor were recorded in all measurements when the nanofiber sensor PAN-RHE was alternately exposed to target vapor. The real-time QCM kinetic measurements for the nanofiber sensor PAN-RHE was recorded during the exposure of the increasing content of the selected vapors between 25 % and 100 % concentration ratios. The results are presented in Fig. 5. When obtaining these kinetic characteristics, the nanofiber sensor PAN-RHE was exposed to dry air first, causing no shifts in resonance frequency, followed by a selected vapor exposure and then re-exposure to dry air. The time interval for each measurement was chosen as 2 min for each cycle.

Time dependent Δf in Fig. 5a for the nanofiber sensor PAN-RHE against acetone and ethanol vapors exhibited a sharp increase in resonance frequency for a few seconds and then the rate of the decrease in Δf slowed down until reaching a nearly saturation at the later stage of VOC vapor adsorption process. It is also clear that when the dry air was injected into the gas cell, desorption of vapor molecules occurred from the nanofiber sensor PAN-RHE until full removal of adsorbed vapor molecules. After that the nanofiber sensor PAN-RHE was fully recovered and ready for another measurement. The similar process for acetone and ethanol vapors was taken at other concentration values. The responses of the nanofiber sensor PAN-RHE were fast and reversible for both vapors. The response and the recovery times were about a few seconds and the recovery was complete. The inset in Fig. 5a indicates the QCM kinetic measurement of Δf versus time at the same concentration value to test the reproducibility of the nanofiber sensor PAN-RHE. Upon injection of vapors, the nanofiber sensor PAN-RHE exhibited similar responses for each cycle. These similar measurements proved that the adsorption processes between the nanofiber sensor PAN-RHE and both vapors were reversible and reproducible.

The Fig. 5b shows Δf values at the different concentrations of acetone and ethanol in three dimensions. As the concentration value increased in both organic vapors, the Δf response values of the nanofiber sensor PAN-RHE also increased. It was observed that the acetone responses at all concentrations were higher than those of ethanol vapor. It was concluded that the sensor is more selective towards acetone than ethanol vapor. The sensitivity value, which is related to the selectivity parameter, was obtained and detailed in this section.

Reproducibility was tested via three reciprocal exposures of the vapor molecules onto the nanofiber sensor PAN-RHE. The inset in Fig. 5a indicates the QCM kinetic measurement of Δf versus time at the same concentration value to test the reproducibility of the nanofiber sensor PAN-RHE. The Fig. 5c gives Δf values of the nanofiber sensor PAN-RHE at the constant concentration of acetone and ethanol vapors. The Δf values taken for acetone are almost equally acceptable. A similar situation was also observed in ethanol vapor, however a decrease in the first measurement was observed. It can be concluded that the nanofiber sensor PAN-RHE has a reproducible response in both vapors.

As presented in Fig. 5c, similar amount of response was obtained during the exposure of the saturated concentration of the gas molecules which indicates the stable PAN-RHE sensor. Moreover, with the injection of the dry air, after the recovery, the baseline stands for the same resonance frequency value. The nanofiber sensor PAN-RHE was stable for the ethanol and acetone exposures. Benzene vapor response given in Fig. S1 depending on time is quite unstable. Although it increased slightly with the increase in concentration values, the response amount decreased rapidly and even fell below the baseline in some cases. It is clear that the benzene vapor interaction of the nanofiber sensor PAN-RHE is unstable. It can be concluded that the nanofiber sensor PAN-RHE is not a good candidate material for benzene vapor detection.

Using Eq. (3), c values were calculated for acetone and ethanol vapors and they were used to determine the sensor sensitivity (S), limit of detection (LOD) and limit of quantification (LOQ). Calibration curve graphs given in Fig. 6 were obtained by plotting Δf against c. A linear fitting was applied to these data to get parameters such as the slope and the correlation coefficient (R^2). The slope of the calibration curve was used to obtain the sensitivity value of the nanofiber sensor PAN-RHE against the selected vapor. S is defined as:

$$S = \frac{\Delta f}{c} \tag{4}$$

in terms of Hz/ppm. The S and R^2 values presented in Table 1of the nanofiber sensor PAN-RHE were determined using Eq. (4) and Fig. 6. R^2

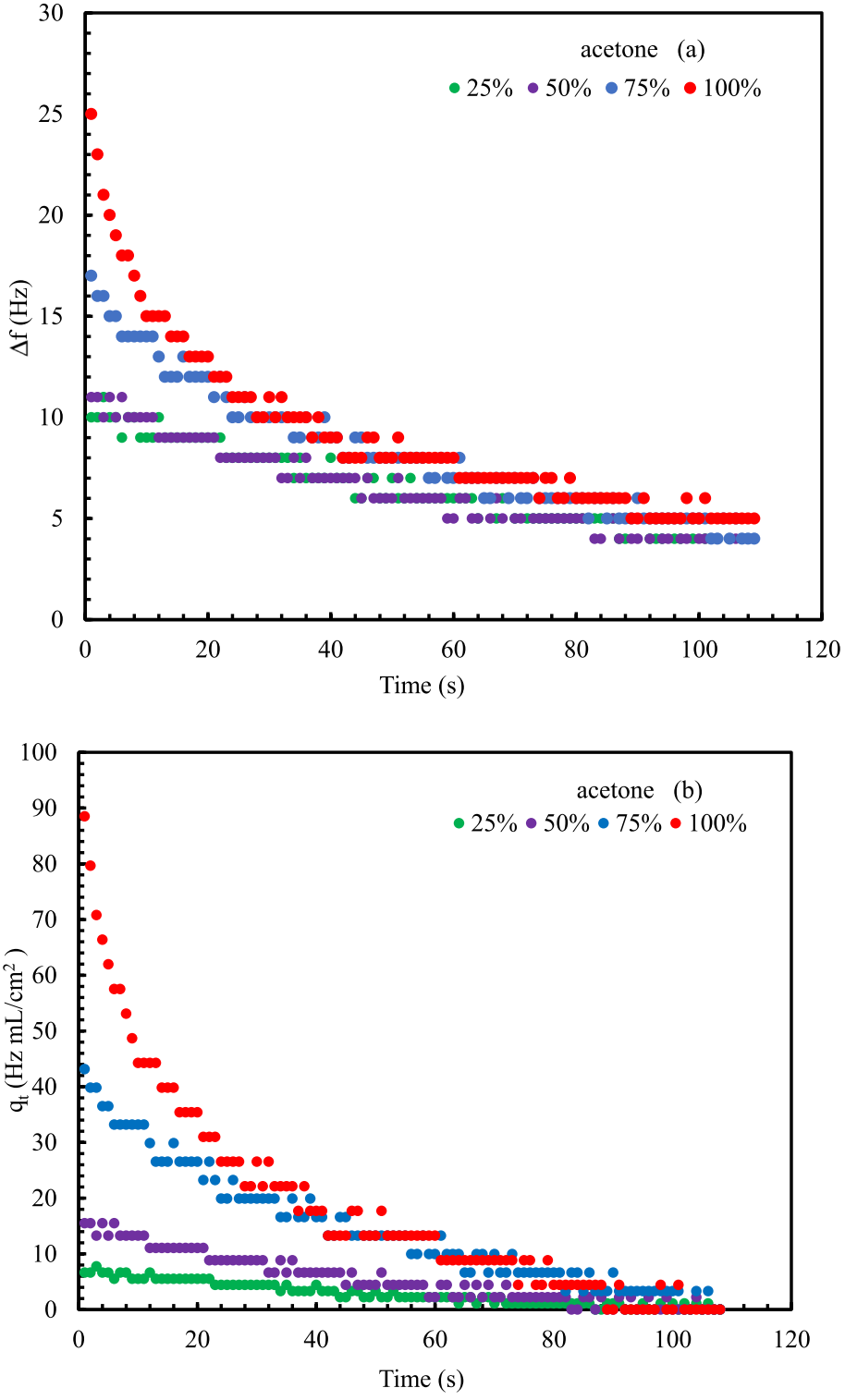

Fig. 7. (a) Δf versus time (b) q_e versus time.

value of acetone vapor is higher than R^2 value of ethanol vapor.

For a sensor material, it is considered to have low *LOD* and *LOQ* values, indicating its higher sensitivity and precision [21]. *LOD* and *LOQ* parameters refer to the lowest amount of a vapor and to the lowest amount accurately quantified respectively. They were described as [42,43]:

$$LOD = \frac{3.3\sigma}{S} \quad (5)$$

$$LOQ = \frac{10\sigma}{S} \quad (6)$$

where σ is the standard deviation and S is the sensitivity value. The σ of the blank measurement is determined by measuring the response of the sensor in the absence of the target VOC molecule (for our case 1 Hz). The calculated *LOD* and *LOQ* values were given in Table 1.

The results of these three studies using the nanofiber sensor PAN-RHE can be summarized as follows: i. the nanofiber sensor PAN-RHE

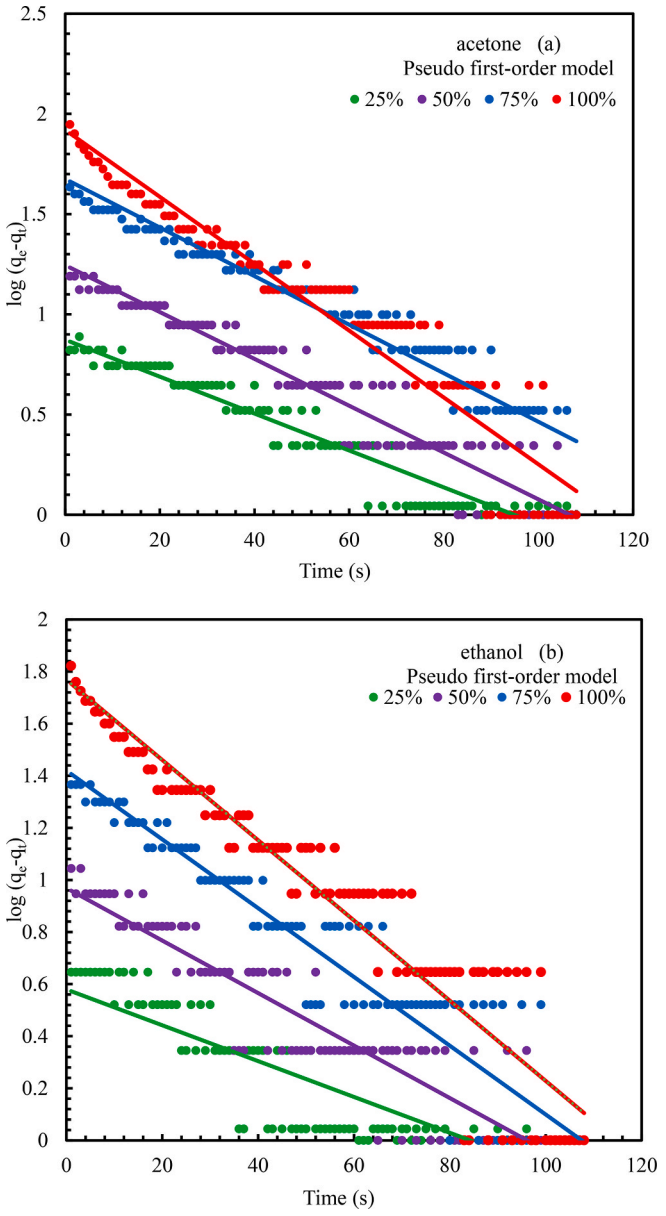

Fig. 8. The fittings for the Pseudo first-order model (a) acetone (b) ethanol.

showed the highest sensitivity, lowest LOD and LOQ values for chloroform vapor, ii. the second highest sensitivity, lowest LOD and LOQ values were produced against acetone vapor, iii. the nanofiber sensor PAN-RHE is not a candidate material for benzene vapor, iv. when the expected sensor parameters for a sensor are evaluated, it is clearly seen from the results that the nanofiber sensor PAN-RHE is a promising nanofiber material for chloroform and acetone sensor materials in the field of room temperature sensor applications.

In the literature, there are very limited studies on QCM based nanofiber sensor fabricated by electrospinning method for an acetone vapor sensor; however, several studied have been published as an acetone vapor sensor materials using different fabrication methods such as spin coating, Langmuir-Blodgett thin film etc. A comparative study [44-48] was made for acetone sensors which were fabricated via different fabrication methods using different materials such as polyacrylonitrile (PAN) nanofibers, N-cyclohexylmethacrylamide, MOF based materials and calix[4]arenes which were presented in Table 2. This study showed a sensitivity of 0.0243 Hz/ppm which is higher than the compared PAN nanofiber study [44] in which LOD and LOQ values were not reported. On the other hand, MOF, calix[4]arene and N-cyclohexylmethacrylamide based sensors showed higher sensitivity compared with this work.

Generally, the frequency shift in the mass sensitive QCM measurements increases linearly with the vapor concentration when more vapor molecules adsorbed onto the sensing material coated on the quartz crystal substrate. This adsorption process depends on the intermolecular forces such as Van-der Waals, hydrogen bonding and dipole–dipole interactions [15,31,42]. These interactions are related to the molar mass, vapor pressure, dipole moment, viscosity parameters and chemical structure of the vapor molecules [49,50].

The sensor applications are strongly related to VOCs properties given in Table 3. The highest sensitivity observed for acetone vapor when compared to ethanol vapor reveals that acetone vapor molecules were introduced onto the nanofiber sensor PAN-RHE more mass deposited because of its high molar mass value. Both vapors have almost the same density. The vapor pressure of acetone vapor is also much higher than of ethanol vapor which could play an important role for surface interaction which contributed to yield a higher frequency shift [51].

Ethanol vapor with a high viscosity yields a lower sensitivity. The lower viscosity of acetone is believed to enhance the sensor's response and recovery characteristics, resulting in a better performance compared to ethanol. The higher dipole moment of ethanol compared to acetone induces stronger electrostatic interactions on polar surfaces of PAN-RHE, facilitating electron transfer. Additionally, acetone's higher dielectric constant relative to ethanol is thought to increase dipole–dipole interactions, thereby accelerating the adsorption processes. The acceleration of response of sensors is attributed to the low viscosity and dipole moment of acetone vapor [52].

Dipole moment for acetone is higher than ethanol which can be explained by dipole–dipole interaction between the nanofiber sensor PAN-RHE and vapor molecules. Ethanol, due to its alcohol group (OH), readily forms strong hydrogen bond with electron donor groups of RHE surface as nitrogen or oxygen species. In contrast, acetone, having a polar carbonyl group, interacts with electron donor groups of the surface less strongly than ethanol. Consequently, this suggests that the adsorption dynamics may be faster when the sensor is exposed to acetone. Additionally, acetone exhibits a higher vapor pressure and a more volatile nature compared to alcohol. The elevated vapor pressure of acetone facilitates faster detection responses. Additionally, acetone's higher volatility contributes to accelerated adsorption processes, thereby enhancing the sensor's response rates [52]. It is also thought that the lower viscosity of acetone improves the response and recovery properties of the sensor, resulting in better performance compared to ethanol. The higher dipole moment of ethanol compared to acetone induces stronger electrostatic interactions on polar surfaces of PAN-RHE, facilitating electron transfer. Additionally, acetone's higher dielectric constant relative to ethanol is thought to increase dipole–dipole interactions, thereby accelerating the adsorption processes. The acceleration of response of sensor is attributed to the low viscosity and dipole moment of acetone vapor.

It can be noted that benzene vapor did not give a stable and noticeable response in this study. It must be stressed that this interaction did not occur for benzene vapor because it has no dipole moment. This part can be concluded that the QCM analysis clearly shows that the sensing mechanism is a dynamic process that occurs in time and that depends on several parameters.

3.4. Adsorption properties of the nanofiber sensor PAN-RHE

To understand the adsorption dynamics, Pseudo first-order and Elovich models were applied to the experimental data taken using QCM measurement. The adsorption capacity or the adsorption amount per unit area (q_t) was described as [23]:

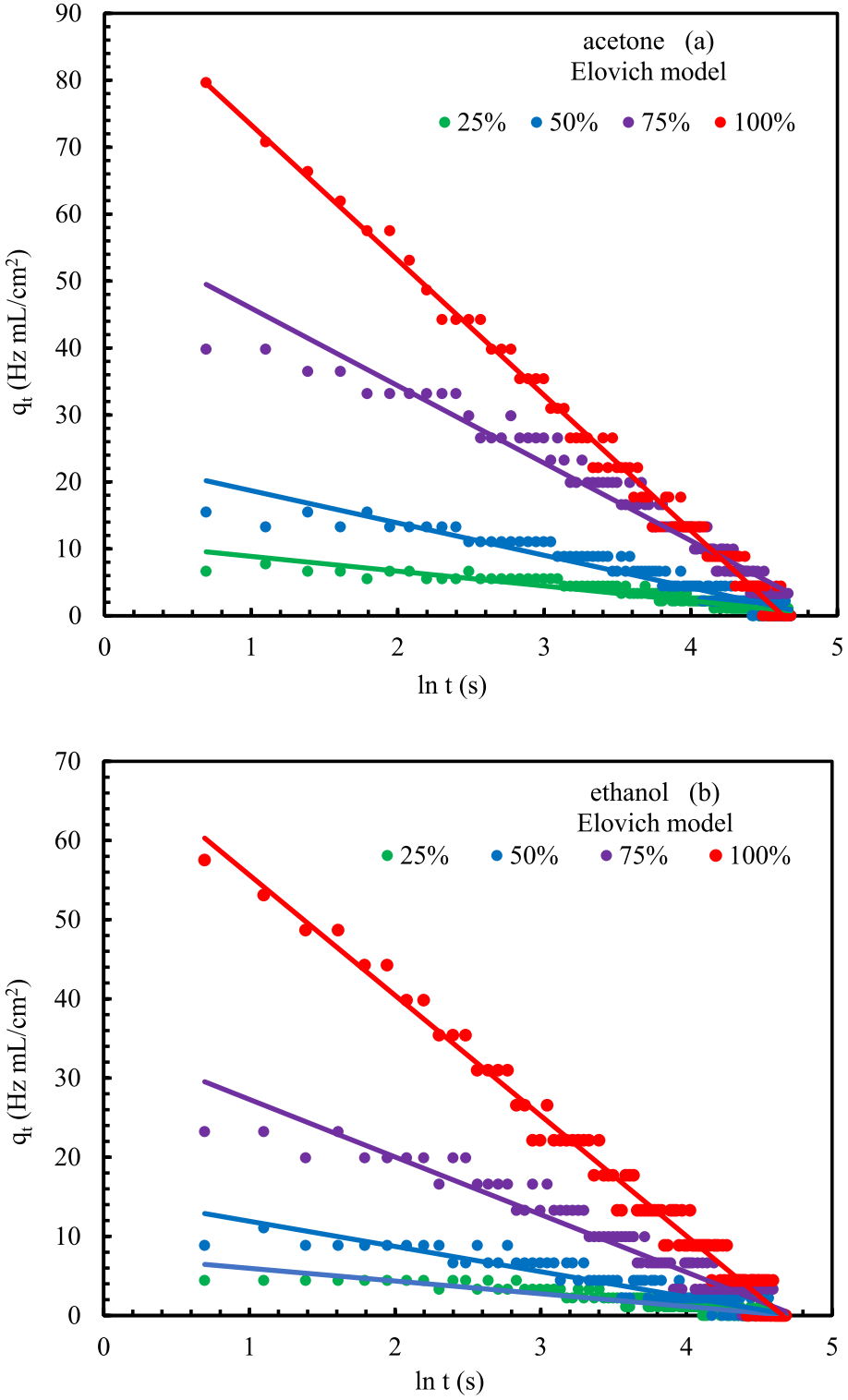

Fig. 9. The fittings for the Elovich model (a) acetone (b) ethanol.

$$q_t = \left[\frac{(q_i - q_e)V}{A}\right] \tag{7}$$

where q_i is the initial frequency, q_t is the equilibrium frequency, A is the surface area which is equivalent to the QCM crystal surface area and V is the injected vapor volume respectively.

Pseudo first-order kinetic equation was given in a linear form as [23]:

$$log(q_e - q_t) = logq_e - \frac{k_1}{2.303}t \tag{8}$$

where q_e is the amount of vapor molecules at equilibrium and q_t is the amount of vapor molecules adsorbed at time t respectively. k_1 is the Pseudo first-order adsorption rate constant.

The Elovich model was described as by [23]:

Table 4
The calculated k_1 and q_e values of the PAN-RHE nanofiber sensor exposed to different concentrations of acetone and ethanol vapors.

concentration	acetone			ethanol		
	k_1(Hz mL/cm^2)	q_e(cm^2 s /Hz mL)	R^2	k_1(Hz mL/cm^2)	q_e(cm^2 s / Hz mL)	R^2
25 %	0.0211	7.4679	0.929	0.0158	3.7983	0.777
50 %	0.0269	17.5832	0.920	0.0232	9.3067	0.875
75 %	0.0278	47.3478	0.911	0.0303	26.2905	0.898
100 %	0.0384	83.1572	0.908	0.0354	58.7218	0.896

$$q_t = \left(\frac{1}{b}\right) ln(ab) + \left(\frac{1}{b}\right) lnt \tag{9}$$

where q_t is the quantity of gas adsorbed at time t, a is the initial adsorption rate and b is the Elovich desorption constant respectively. If we assume $t \gg t_0$, a plot of q_t versus lnt yields a linear relationship.

The nanofiber sensor PAN-RHE was exposed to acetone and ethanol vapors at 4 different concentration values between 25 % and 100 %. QCM kinetic measurements were taken in the form of air-vapor-air-vapor at 2-minute intervals. To understand the adsorption dynamics, Δf values for each concentration were taken from Fig. 5a when the vapor molecules were exposed to the gas cell until dry air was injected to the gas cell. Selected Δf for acetone vapor as a function of time is given in Fig. 7a. The q_e values of the nanofiber sensor PAN-RHE were determined with the help of Eq. (7) and is presented in Fig. 7b.

Similar processes were followed for ethanol vapor. Δf and q_e values against time were given in Fig. S2. The fittings for the Pseudo first-order model [$\log(q_e - q_t) versus t$] and the Elovich model [$q_t versus \ln t$] for acetone and ethanol vapors were given in Figs. 8 and 9 respectively. The slopes of these graphs are useful to calculate the adsorption parameters for both models. The parameters for the Pseudo first-order model were calculated with the help of Eq. (8) and Fig. 8. They were given in Table 4. Similarly, the Elovich model parameters were determined for the nanofiber sensor PAN-RHE using Eq. (9) and Fig. 9. These parameters were given in Table 5.

When they are analyzed, it is seen that the Pseudo first-order adsorption rate constant value of the nanofiber sensor PAN-RHE for acetone vapor is slightly higher than that for ethanol vapor, but the increase is seen more clearly in q_e values. When the fitting parameter R^2 values are compared, it is observed that the R^2 value of acetone vapor is higher than the R^2 value of ethanol vapor for all concentrations.

The value of a for acetone vapor is higher than that of ethanol vapor for each concentration value. This means that the initial adsorption rate is higher for acetone vapor. As the concentration value increases, the a values for both vapors increase and this value for acetone vapor is higher than for ethanol vapor. b values are known as the Elovich desorption constant and the b values in ethanol vapor are higher than for acetone. R^2 values for both vapor cases were obtained as more or less similar. The adsorption coefficients of the nanofiber sensor PAN-RHE calculated using the Pseudo first-order and Elovich models for selected vapors were given in the Table 6.

The results of the two applied models showed that the Pseudo first-order rate constant values (k_1) and the Elovich initial adsorption rate (a) both give information on the adsorption behavior of the gas molecules. These values are higher for acetone vapor compared with that of the ethanol vapor which is compatible with the calculated sensitivity values. The highest value of the amount of vapor molecules adsorbed at equilibrium or equilibrium density (q_e) was found for acetone vapor supports the high sensitivity value. The Elovich desorption constant (b) value of acetone vapor is lower than ethanol vapor indicating the slow desorption of the acetone vapor compared with the ethanol vapor. These results can be summarized that the highest number of adsorbed vapor molecules are for acetone vapor when the nanofiber sensor PAN-RHE reaches equilibrium with vapor molecules. This result is supported with the S value of acetone vapor because of the highest sensitivity of the nanofiber sensor PAN-RHE to acetone vapor.

3.5. Density functional theory calculation and binding mechanisms between the nanofiber sensor PAN-RHE and vapors

To better understand the nature of the binding capability of (PAN-RHE) with acetone vapor and/or ethanol, geometric optimizations and theoretical calculations of rhodamine (RHE) and/or nitrile units of polymer chain (PAN) and their acetone or ethanol interactions were verified by applying density functional theory (DFT) with B3LYP and 6-311G (d,p) basis. DFT calculations were conceded using Gaussian 09 program [29]. The optimized geometries, acetone and ethanol interaction forms were given in Fig. 10.

In the complex interactions, VOC compounds (acetone or ethanol) generally prefer to coordinate with polar groups of RHE by dipole–dipole (for acetone) or hydrogen binding (for ethanol) interaction mechanism. The highest occupied and lowest unoccupied molecular orbitals (LUMO and HOMO) dispersions and energies of complex structure of (PAN-RHE) were calculated. As shown in Fig. 10, the LUMO and HOMO orbitals are located in different parts of (PAN-RHE) complexes. In the case of interaction forms of RHE group of PAN-RHE with acetone, HOMO orbital is primarily dispersed on the two phenyl rings and carbonyl unit of rhodamine. Compared the HOMO and LUMO orbitals, while the orbitals are commonly located both onto the entire molecule of RHE and acetone molecule, the same orbitals are not dispersed on ethanol molecule during the interaction. The energy gaps (Egap) between the LUMO and HOMO of (PAN-RHE) with acetone were 1.48 eV for acetone, whereas the energy gaps for PAN-RHE and ethanol were found to be 4.08 eV, respectively. A large energy gap between HOMO and LUMO implies low stability and chemical reactivity. In turn, a small energy gap implies high stability and chemical reactivity [53]. These calculations indicated that LUMO-HOMO energy gaps of complexes remarkably reduced with decreasing dipole moment values and stabilized the system owing to the possible interaction between PAN-RHE and acetone. Lowest LUMO-HOMO energy gap and dipole moment of acetone among the tested ethanol are responsible for its strongest

Table 6
The adsorption parameters of the nanofiber sensor PAN-RHE exposed to VOCs.

concentration (100 %)	Pseudo first-order		Elovich	
	k_1(Hz mL/cm^2)	q_e(cm^2 s/Hz mL)	a(Hz mL/cm^2)	b(cm^2 s /Hz mL)
Acetone	0.0384	83.1572	2069.4312	0.0494
Ethanol	0.0354	58.7218	1607.2268	0.0658

Table 5
The constants a and b of the nanofiber sensor PAN-RHE exposed to different concentrations of acetone and ethanol vapors.

concentration	acetone			ethanol		
	a(Hz mL/cm^2)	b(cm^2 s /Hz mL)	R^2	a(Hz mL/cm^2)	b(cm^2 s /Hz mL)	R^2
25 %	331.2205	0.4518	0.876	178.8068	0.6223	0.851
50 %	628.4891	0.2069	0.908	364.5375	0.3141	0.877
75 %	1665.2093	0.0863	0.948	843.4460	0.1374	0.930
100 %	2069.4312	0.0494	0.988	1607.2268	0.0658	0.981

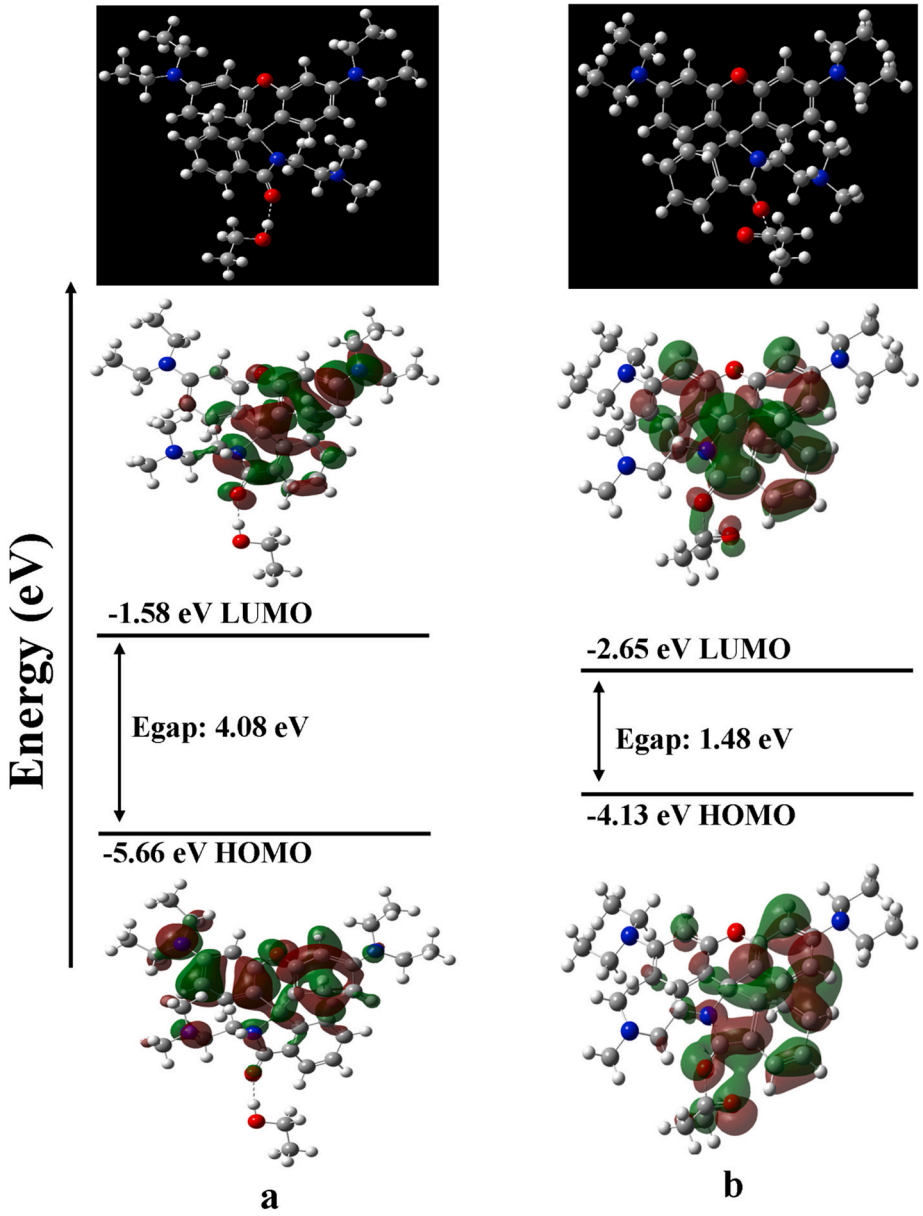

Fig. 10. Energy diagrams of HOMO and LUMO orbitals; (a) RHE-Ethanol, (b) RHE-acetone complexes.

sensing response [54]. Therefore, theoretical data are in agreement with the obtained sensor results.

Furthermore, the sensitivity and binding mechanism of the QCM sensor to acetone or ethanol molecules are related to the interaction between the binding layer and acetone/ethanol molecules. The possible interaction between the QCM layer and the vaporized analyte molecules (acetone or ethanol) can be associated with sorption capabilities of acetone and/or ethanol molecules with the nitrile or rhodamine units of nanofiber mat (RHE-PAN) belonging to QCM surface. This possible interaction between the vaporized analytes and the surface of the sensor is referred to the weak interaction forces including π-π interactions, hydrogen bonding, dipole–dipole bonding or electrostatic attractions. With the help of one or a combination of these molecular forces, vaporized analytes most probably formed powerful noncovalent adsorption with the QCM surface. Hydrogen bonding or dipole–dipole interactions [55–57] are the basic molecular mechanism during the sensing process. Fig. 11 shows the possible hydrogen binding or dipole–dipole interaction between the ethanol or acetone molecule with rhodamine and/or nitrile units of the PAN fiber chain. While carbonyl groups of rhodamine and/or nitrile units of the PAN fiber can be considered as a hydrogen acceptor for vaporized ethanol, same units of PAN surface act as dipole forces which are attractive forces between the positive end of one vaporized acetone molecule and the negative (lone pairs) end of another molecule.

4. Conclusions

The nanofiber sensor PAN-RHE was tested against acetone, ethanol, and benzene vapors for sensor applications at 25 °C. The sensor response was found to be sensitive, stable, reproducible and concentration dependent to acetone and ethanol vapors. On the other hand, it did not show a stable response to benzene vapor. Acetone vapor showed a good response with a sensitivity (0.0243 Hz/ppm), a low limit of detection (135.80 ppm) and a low limit of quantification (411.52 ppm) respectively. The Pseudo first-order adsorption rates were increasing and Elovich desorption constants were decreasing when the vapor concentrations increased. Hydrogen binding or dipole–dipole interaction played an important role between vapor molecules with rhodamine

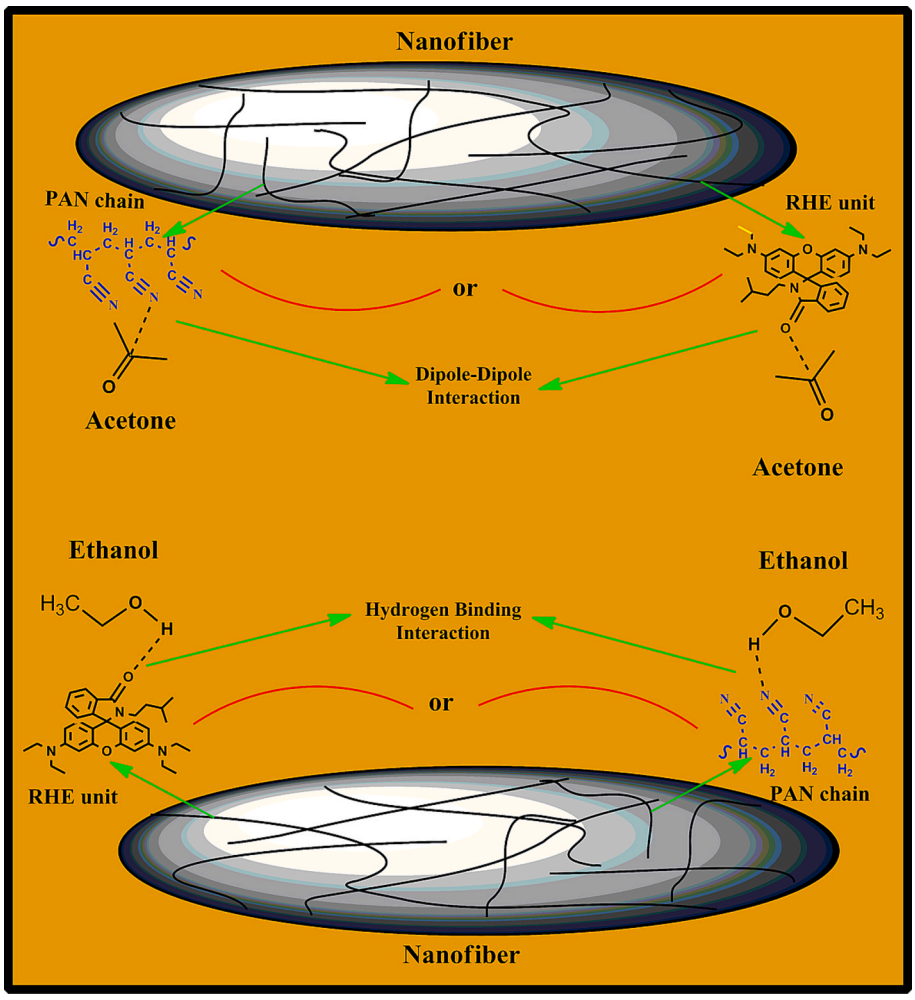

Fig. 11. Molecular structures and possible binding mechanisms between targeted volatile acetone and/or ethanol molecules and PAN-RHE fiber chains.

and/or nitrile units of the PAN fiber chain. Finally, it is clearly seen from the results that the nanofiber sensor PAN-RHE is a promising nanofiber material for acetone vapor in the field of room temperature sensor applications.

CRediT authorship contribution statement

Rifat Capan: Writing – review & editing, Writing – original draft, Visualization, Validation, Supervision, Project administration, Methodology, Investigation, Formal analysis, Data curation, Conceptualization. **Inci Capan:** Writing – review & editing, Writing – original draft, Visualization, Methodology, Formal analysis, Data curation, Conceptualization. **Mevlut Bayrakci:** Writing – review & editing, Writing – original draft, Validation, Methodology, Investigation, Formal analysis, Data curation, Conceptualization.

Declaration of competing interest

The authors declare that they have no known competing financial interests or personal relationships that could have appeared to influence the work reported in this paper.

Appendix A. Supplementary data

Supplementary data to this article can be found online at https://doi.org/10.1016/j.mseb.2025.118581.

Data availability

The authors do not have permission to share data.

References

[1] I.C. Ossai, F.S. Hamid, S.C.A. Mana, A. Hassan, Ecotoxicological effects, human and animal health risks of pollution and exposure to waste engine oils: a review, Environ. Geochem. Health 46 (2024) 416, https://doi.org/10.1007/s10653-024-02198-7.

[2] L. Copolovici, A.C. Popitanu, D.M. Copolovici, Volatile organic compound emission and residual substances from plants in light of the globally increasing CO_2 level, Cur. Opinion Environ. Sci. Health 19 (2021) 100216, https://doi.org/10.1016/j.coesh.2020.10.004.

[3] K. Kim, S. Lee, Y. Choi, D. Kim, Emissions of fungal volatile organic compounds in residential environments and temporal emission patterns: implications for sampling methods, Int. J. Environ. Res. Public Health 19 (2022) 12601, https://doi.org/10.3390/ijerph191912601.

[4] D. Meheust, P.L. Cann, G. Reboux, L. Millon, J.P. Gangneux, Indoor fungal contamination: health risks and measurement methods in hospitals, homes and workplaces, Crit. Rev. Microbiol. 40 (2014) 248–260, https://doi.org/10.3109/1040841X.2013.777687.

[5] A. Jalal, F. Alam, S.R. Choudhury, Y. Umasankar, N. Pala, S. Bhansali, Prospects and challenges of volatile organic compound (VOC) sensors in human healthcare, ACS Sens. 3 (2018) 1246–1263, https://doi.org/10.1021/acssensors.8b00400.

[6] P.F. Infante, Benzene and leukemia: the 0.1 ppm ACGIH proposed threshold limit value for benzene, Appl. Occupat. Environ. Hygiene 7(4) (1992) 253–262, https://doi.org/10.1080/1047322X.1992.10389769.

[7] A. Mirzaei, S.G. Leonardi, G. Neri, Detection of hazardous volatile organic compounds (VOCs) by metal oxide nanostructures-based gas sensors: a review, Cer. Internat. 42 (2016) 15119–15141, https://doi.org/10.1016/j.ceramint.2016.06.145.

[8] G.X. Ma, Z. Wei, R. Husni, P. Do, K. Zhou, J. Rhee, Y. Tan, K. Navder, M.C. Yeh, Characterizing occupational health risks and chemical exposures among asian nail

salon workers on the east coast of the United States, J. Com. Health 44 (2019) 1168–1179, https://doi.org/10.1007/s10900-019-00702-0.
[9] J.J. Keenan, S. Gaffney, S.A. Gross, C.J. Ronk, D.J. Paustenbach, D. Galbraith, B. D. Kerger, An evidence-based analysis of epidemiologic associations between lymphatic and hematopoietic cancers and occupational exposure to gasoline, Human & Exper. Toxic. 32 (10) (2013) 1007–1027, https://doi.org/10.1177/0960327113476909.
[10] F. Gu, L. Zhang, S. Hong, D. Han, Z. Wang, Atomically dispersed rhodium on ordered macroporous In2O3 for highly sensitive detection of ethanol and the sensing mechanism, J. Mat. Chem. C 11 (18) (2023) 5995–6003, https://doi.org/10.1039/D3TC00534H.
[11] E. David, V.C. Niculescu, Volatile organic compounds (VOCs) as environmental pollutants: occurrence and mitigation using nanomaterials, Int. J. Environ. Res. Public Health 18 (2021) 13147, https://doi.org/10.3390/ijerph182413147.
[12] A. Bag, N.E. Lee, Gas sensing with heterostructures based on two dimensional nanostructured materials: a review, J. Mater. Chem. C 7 (2019) 13367–13383, https://doi.org/10.1039/C9TC04132J.
[13] N. Bu, Y. Yan, X. Chen, X. Bai, Z. Tong, Liquid crystal gel-based acetone sensor using correlated laser speckles, Sens. Act. b. Chem. 423 (2025) 136773, https://doi.org/10.1016/j.snb.2024.136773.
[14] N.L. Torada, J. Kim, M. Kim, H. Lim, J. Na, S.M. Alshehri, T. Ahamad, Y. Yamauchi, M. Eguchi, B. Ding, X. Zhang, Nanoarchitectured porous carbons derived from ZIFs toward highly sensitive and selective QCM sensor for hazardous aromatic vapors, J. Hazardous Mat. 405 (2021) 124248, https://doi.org/10.1016/j.jhazmat.2020.124248.
[15] R. Sukowati, Y.M. Rohman, B.H. Agung, D.A. Hapidin, H. Damayanti, K. Khairurrijal, An investigation of the influence of nanofibers morphology on the performance of QCM-based ethanol vapor sensor utilizing polyvinylpyrrolidone nanofibers active layer, Sens. Act. B Chem. 386 (2023) 133708, https://doi.org/10.1016/j.snb.2023.133708.
[16] A. Rianjanu, F. Fauzi, K. Triyana, H.S. Wasisto, Electrospun nanofibers for quartz crystal microbalance gas sensors: a review, ACS Appl. Nano Mater. 4 (10) (2021) 9957–9975, https://doi.org/10.1021/acsanm.1c01895.
[17] A.I. Yardimci, N. Yagmurcukardes, M. Yagmurcukardes, I. Capan, M. Erdogan, R. Capan, O. Tarhan, Y. Acikbas, Electrospun polyacrylonitrile (PAN) nanofiber: preparation, experimental characterization, organic vapor sensing ability and theoretical simulations of binding energies, Appl. Phys. A 128 (2022) 173, https://doi.org/10.1007/s00339-022-05314-5.
[18] N. Yagmurcukardes, A.I. Yardimci, M. Yagmurcukardes, I. Capan, M. Erdogan, R. Capan, Y. Acikbas, Electrospun polyacrylonitrile (PAN)/polypyrrole (PPy) nanofber–coated quartz crystal microbalance for sensing volatile organic compounds, J. Mater. Sci. Mater. Electron. 34 (2023) 1869, https://doi.org/10.1007/s10854-023-11281-1.
[19] M. Febrina, A. Rianjanu, A. Rajak, R.R. Mukti, M. Djamal, Electrospun polyacrylonitrile nanofibers mixed with citric acid as a quartz crystal microbalance ammonia vapor sensor, ChemistrySelect 7 (2022) e202103615, https://doi.org/10.1002/slct.202103615.
[20] A. Rianjanu, K. Triyana, N. Nurbaiti, S.A. Hasanah, A. Kusumaatmaja, R. Roto, An enhanced safrole sensing performance of a polyacrylonitrile nanofiber-based-QCM sensor by overlaying with chitosan, Sains Malays. 48 (9) (2019) 2041–2049, https://doi.org/10.17576/jsm-2019-4809-25.
[21] Y.M. Rohman, R. Sukowati, A. Priyanto, D.A. Hapidin, D. Edikresnha, K. Khairurrijal, Quartz crystal microbalance coated with polyacrylonitrile/nickel nanofibers for high-performance methanol gas detection, ACS Omega 8 (2023) 13342–13351, https://doi.org/10.1021/acsomega.3c00760.
[22] R. Capan, I. Capan, M. Bayrakci, Rhodamine-based electrospun polyacrylonitrile (PAN) nanofiber sensor for the detection of chlorinated hydrocarbon vapors, ACS Appl. Polym. Mater. 6 (2024) 7500–7511, https://doi.org/10.1021/acsapm.4c00909.
[23] R. Capan, I. Capan, M. Bayrakci, Sensor parameters and adsorption behaviour of rhodamine-based polyacrylonitrile (PAN) nanofiber against dichloromethane vapour, Microchem. J. 207 (2024) 111806, https://doi.org/10.1016/j.microc.2024.111806.
[24] F. Temel, One novel calix[4]arene based QCM sensor for sensitive, selective and high performance-sensing of formaldehyde at room temperature, Talanta 211 (2020) 120725, https://doi.org/10.1016/j.talanta.2020.120725.
[25] R. Capan, I. Capan, F. Davis, A new approach for the adsorption kinetics using surface plasmon resonance results, Sens. Act. B Chem. 394 (2023) 134463, https://doi.org/10.1016/j.snb.2023.134463.
[26] A. Rianjanu, S.N. Hidayat, T. Julian, E.A. Suyono, A. Kusumaatmaja, K. Triyana, Swelling behavior in solvent vapor sensing based on quartz crystal microbalance (QCM) coated polyacrylonitrile (PAN) nanofiber, IOP Conf. Ser.: Mater. Sci. Eng. 367 (2018) 012020, https://doi.org/10.1088/1757-899X/367/1/012020.
[27] B. Niu, Z. Zhai, J. Wang, C. Li, Preparation of ZIF-8/PAN composite nanofiber membrane and its application in acetone gas monitoring, Nanotechnology 34 (2023) 245710, https://doi.org/10.1088/1361-6528/acc4ca.
[28] Z. Zhai, Y. Sun, X. Hao, C. Li, Capacitive gas sensors based on a ZIF-67/PAN nanofiber membrane to detect volatile organic compounds, Appl. Surf. Sci. 621 (2023) 156833, https://doi.org/10.1016/j.apsusc.2023.156833.
[29] Z. Aydin, M. Keskinates, B. Yilmaz, M. Bayrakci, An isonicotinohydrazide based fluorescence sensor for detection of Zn^{2+} in biological systems: experimental and theoretical studies along with cell imagine, Inorg. Chim. Acta 557 (2023) 121680, https://doi.org/10.1016/j.ica.2023.121680.
[30] G. Sauerbrey, Verwendung von schwingquarzen zur wägungdünner schichten und zur mikrowägung, Zeitschrift Für Physik 155 (1959) 206–222, https://doi.org/10.1007/BF01337937.
[31] A. Rianjanu, K. Triyana, D.B. Nugroho, A. Kusumaatmaja, R. Roto, Electrospun polyvinyl acetate nanofiber modified quartz crystal microbalance for detection of primary alcohol vapor, Sens. Actuators a: Phys. 301 (2020) 111742, https://doi.org/10.1016/j.sna.2019.111742.
[32] L. Katriani, R. Aflaha, A.H. As'ari, P. Nurwantoro, R. Roto, K. Triyana, Nanofiber-coated quartz crystal microbalance with chitosan overlay for highly sensitive room temperature ammonia gas sensor, Microchem. J. 206 (2024) 111532, https://doi.org/10.1016/j.microc.2024.111532.
[33] X. Fan, B.Y. Du, Selective detection of trace p-xylene by polymer-coated QCM sensors, Act. B 166 (2012) 753–760, https://doi.org/10.1016/j.snb.2012.03.060.
[34] H. Borsdorf, P. Fiedler, T. Mayer, The effect of humidity on gas sensing with ion mobility spectrometry, Sens. Act. B Chem. 218 (2015) 184–190, https://doi.org/10.1016/j.snb.2015.04.102.
[35] M. Asgari, F.H. Saboor, S.P. Amouzesh, M.W. Coull, A.A. Khodadadi, Y. Mortazavi, T. Hyodo, Y. Shimizu, Facile ultrasonic-assisted synthesis of SiO 2 /ZnO core/shell nanostructures: a selective ethanol sensor at low temperatures with enhanced recovery, Sens. Act. B Chem. 368 (2022) 132187, https://doi.org/10.1016/j.snb.2022.132187.
[36] T. Hyodo, K. Urata, K. Kamada, T. Ueda, Y. Shimizu, Semiconductor-type SnO based NO 2 2- sensors operated at room temperature under UV-light irradiation, Sens. Act. B Chem. 253 (2017) 630–640, https://doi.org/10.1016/j.snb.2017.06.155.
[37] E. Hoviezi, S. Mojezi–badil, Z. Ansari-Asl, Fabrication, characterization, and biocompatibility assessment of polycaprolactone/polyacrylonitrile/casein nanofibers scaffold for tissue engineering applications, Fibers and Polym. 26 (2025) 1075–1089, https://doi.org/10.1007/s12221-025-00859-7.
[38] Z. Khan, F. Kafiah, H.Z. Shafi, F. Nufaiei, S.A. Furquan, A. Matin, Electrospun polyacrylonitrile (PAN) nanofiber mats *(PDF) morphology, mechanical properties and Surface Characteristics of electrospun polyacrylonitrile (PAN) nanofiber Mats*. Inter. J. Adv. Eng. Nano Tech. (IJAENT) 2 (3) (2015) 15–22. ISSN: 2347-6389.
[39] A. Rianjanu, M. Aulya, M.A.A.P. Rayhan, R. Aflaha, S. Maulana, T. Taher, W. S. Sipahutar, M.I. Maulana, N. Yulianto, K. Triyana, H.S. Wasisto, Impact of hydrophilic bamboo cellulose functionalization on electrospun polyacrylonitrile nanofiber-based humidity sensors, MRS Commun. 13 (3) (2023) 514–519, https://doi.org/10.1557/s43579-023-00367-w.
[40] Z. Li, M. Teng, R. Yang, F. Lin, Y. Fu, W. Lin, J. Zheng, X. Zhong, X. Chen, B. Yang, Y. Liao, Sb-doped WO3 based QCM humidity sensor with self-recovery ability for real-time monitoring of respiration and wound, Sens. Act. B Chem. 361 (2022) 131691, https://doi.org/10.1016/j.snb.2022.131691.
[41] V.C. Gonçalves, D.T. Balogh, Optical chemical sensors using polythiophene derivatives as active layer for detection of volatile organic compounds, Sens. Act. B Chem. 162 (2012) 307–312, https://doi.org/10.1016/j. snb.2011.12.084.
[42] K. Triyana, A. Rianjanu, D.B. Nugroho, A.H. Asari, A. Kusumaatmaja, R. Roto, R. Suryana, H.S. Wasisto, A highly sensitive safrole sensor based on polyvinyl acetate (PVAc) nanofiber-coated QCM, Sci. Rep. 9 (2019) 15407, https://doi.org/10.1038/s41598-019-51851-0.
[43] A. Mollahosseinia, Y. Elyasia, M. Rastegari, Flat membrane-based electromembrane extraction coupled with UV-visible spectrophotometry for the determination of diethylhexyl phthalate in water samples, Microchem. J. 151 (2019) 104191, https://doi.org/10.1016/j.microc.2019.104191.
[44] A.H. Asari, R. Aflaha, L. Katriani, A. Kusumaatmaj, R. Yudianti, K. Triyana, Investigation of the multiple doping of citric acid and chitosan in nanofiber for enhancement of a quartz crystal microbalance–based ammonia sensor, J. Elect. Mat. 54 (2025) 1678–1690, https://doi.org/10.1007/s11664-024-11646-0.
[45] E. Haghighi, S. Zeinali, A highly sensitive toluene and xylene QCM nanosensor using nanoporous MIL-101(Cr) as a sensing layer, ChemistrySelect 8 (18) (2023) e202204307, https://doi.org/10.1002/slct.202204307.
[46] E. Haghighi, S. Zeinali, Formaldehyde detection using quartz crystal microbalance (QCM) nanosensor coated by nanoporous MIL-101(Cr) film, Microporous and Mesoporous Mater. 300 (2020) 110065, https://doi.org/10.1016/j.micromeso.2020.110065.
[47] M. Durmaz, Y. Acikbas, S. Bozkurt, R. Capan, M. Erdogan, C. Ozkaya, A novel calix [4]arene thiourea decorated with 2-(2 aminophenyl)benzothiazole moiety as highly selective chemical gas sensor for dichloromethane vapor, ChemistrySelect 6 (19) (2021) 4670–4676, https://doi.org/10.1002/slct.202100631.
[48] Y. Acikbas, R. Capan, M. Erdogan, N. Cankaya, C. Soykan, Characterization of N-cyclohexylmethacrylamide LB thin films for room temperature vapor sensor application, J. Macromol. Sci. A 53 (3) (2016) 132–139, https://doi.org/10.1080/10601325.2016.1132907.
[49] L. Xu, X. Hu, Y.T. Lim, V.S. Subramanian, Organic vapor adsorption behavior of poly(3-butoxythiophene) LB films on quartz crystal microbalance, Thin Solid Films 417 (2002) 90–94, https://doi.org/10.1016/S0040-6090(02)00634-X.
[50] V. Yılmaz, N. Can, A. Altındal, Adsorption of VOC vapors on ZnPc: sensing and kinetic studies, Environ. Sci. Pollut. Res. (2024) 1–13, https://doi.org/10.1007/s11356-024-35576-w.
[51] I. Capan, M. Erdogan, G.A. Stanciu, S.G. Stanciu, R. Hristu, M. Göktepe, The interaction between the gas sensing and surface morphology properties of LB thin films of porphyrins in terms of the adsorption kinetics, Mater. Chem. Phys. 136 (2012) 1130–1136, https://doi.org/10.1016/j.matchemphys.2012.08.064.
[52] A.N. Şahin, A. Altındal, Z.G. Özdemir, Acetone and isopropyl alcohol vapor sensing properties of NiO films under varying bias voltages at room temperature, Phys. Status Solidi A Appl. Mater. Sci. 222 (11) (2025) 2400891, https://doi.org/10.1002/pssa.202400891.
[53] Y. Ruiz-Morales, HOMO-LUMO gap as an index of molecular size and structure for polycyclic aromatic hydrocarbons (PAHs) and asphaltenes: a theoretical study. I,

J. Phys. Chem. 106 (46) (2020) 11283–11308, https://doi.org/10.1021/jp021152e.
[54] M.M. Rahman, S. Roy, Adsorption properties of acetone, acetoacetic acid and beta-hydroxybutyric acid on arm chair(8,8)gallium nitride nanotube: a density functional theory approach, Results Surf. Interfaces 3 (2021) 100012, https://doi.org/10.1016/j.rsurfi.2021.100012.
[55] X. Liang, J. Chi, Z. Yang, The influence of the functional group on activated carbon for acetone adsorption property by molecular simulation study, Microporous and Mesoporous Mater. 262 (2018) 77–88, https://doi.org/10.1016/j.micromeso.2017.06.009.
[56] X. Yu, S. Liu, G. Lin, X. Zhu, S. Zhang, R. Qu, C. Zhenga, X. Gao, Insight into the significant roles of microstructures and functional groups on carbonaceous surfaces for acetone adsorption, RSC Adv. 8 (2018) 21541–21550, https://doi.org/10.1039/C8RA03099E.
[57] M. Bayrakcı, Ş. Ertul, M. Yilmaz, Transportation of poorly soluble drug molecules from the organic phase to the aqueous phase by using phosphorylated calixarenes, J. Chem. Eng. Data 56 (12) (2011) 4473–4479, https://doi.org/10.1021/je2004319.